

Compressive Sampling Multispectral Imaging and Unmixing Method for Fluorescent Imaging

Yamin Song¹, Fuhong Cai¹, Julian Evans¹, Erik Forsberg^{1, *}, and Sailing He^{1, 2}

Abstract—Multispectral imaging is an important tool for understanding composite materials in many disciplines. Spectral unmixing enables the determination of individual fluorophore distributions. Due to the dispersive nature of biomaterials the observed spectra of fluorescent dyes is unknown. Spectral unmixing can be accomplished for unknown endmember spectra using minimum volume simplex analysis (MVSA). Compressive sampling (CS) is a method to reduce the computational cost of operating on sparse data sets and can be performed efficiently using NESTA based on Nesterov’s algorithm. Here we demonstrate that NESTA and MVSA can be combined with a denoising threshold to create a compressive sampling and multispectral unmixing (CSMIU) method that enables efficient bioimaging and unmixing with high levels of accuracy (spectral angle distances (SADs) < 0.05). This CSMIU method may potentially enable broadband and *in vivo* bioimaging modalities.

1. INTRODUCTION

Multispectral imaging (MSI) is an important tool to acquire a spectral image and has a wide range of practical applications, including identification of orbital debris [1], astrophysical spectroscopy [2], and biomedical imaging [3]. Combining with the spectral unmixing method, the wealth of spectral information in a 2-D image allows for auto identification in the spectral-image [4]. Spectral unmixing is an important method for *in vivo* fluorescence imaging [5, 6]. Typically, an imaging spectrometer or a liquid crystal tunable filter (LCTF) acts as dispersive element in an MSI system and a 2-D Charge Coupled Device (CCD) captures the optical signal [7]. Si-based CCDs, which are relatively cheap and commonly used, are useable in the spectral range between 200 nm–1100 nm. Unfortunately however, imaging at wavelengths outside this spectral range is significantly more complicated and costly [8].

An imaging method using a single-pixel detector and a Digital Mirror Device (DMD) to acquire an image [6], can be a reasonably efficient and cheap to acquire a signal in a spectral range much broader than that with Si-based CCD. In principle, by substituting the single-pixel detector with a proper monochromator, a single-pixel imaging system can work from the visible to the infrared (450 nm–2500 nm). However, current single-pixel imaging systems are limited by their achievable frames per second (fps) rate due to the modulation frequency of the DMD. Compressive sampling (CS) is an efficient signal acquisition protocol that is able to reconstruct the signal from an apparent incomplete set of measurements by utilizing the fact that many natural signals are sparse or compressible when expressed in a proper function basis [9]. The object reconstruction can be achieved by solving a convex optimization program [10].

In Ref. [11], a CS based imaging method was applied to separate the different zone of a color wheel presented. However the algorithm used requires certain a priori knowledge about the endmembers (being the spectrum of distinct materials of which a mixed pixel is composed).

Received 14 January 2016, Accepted 14 February 2016, Scheduled 19 February 2016

* Corresponding author: Erik Forsberg (erik.forsberg@jorcep.org).

¹ Centre for Optical and Electromagnetic Research, Zhejiang Key Laboratory of Sampling Technologies, Zhejiang University, Hangzhou 310058, China. ² Department of Electromagnetic Engineering, Royal Institute of Technology, Stockholm 10044, Sweden.

Here we report a compressive sampling multispectral imaging method, in which blind spectral unmixing without knowing the endmember distributions a priori is achieved. We show that through properly removing the noise in raw data, the multispectral images derived from compressive sampling can be well unmixed without a priori knowledge of the spectral information of fluorescent agents under investigation.

2. METHODS

2.1. Multispectral Unmixing

In multispectral imaging the spectrum of each pixel represents a mixture of the spectra of the distinct materials (endmembers). By using a multispectral unmixing method, the measured spectrum of such a mixed pixel can be decomposed into the distinct spectra of the endmembers and their fractional abundances (the relative concentration of the endmembers in the pixel) can be obtained [12].

The linear spectral mixture model (LSMM) is one of the commonly used approaches to analyze multispectral images and unmix a measured spectrum of several different material substances. In LSMM, it is assumed that the spectral response in each pixel is a linear combination of the individual spectra of luminophor materials:

$$Y = cMX = c \sum_{i=1}^p M_i X_i, \quad (1)$$

where Y is the raw experimental multispectral image with dimension of $L \times N$; L is the number of bands; N is the number of pixels; p is the number of luminophor materials. $M(X)$ is an $L \times p$ ($p \times N$) matrix representing the respective materials spectra (concentration distributions); M_i is the i th column vector of M describing the spectrum of the i th material; X_i is the i th row vector of X describing the i th material's concentration distribution; c is a constant coefficient.

In our study, we use the MVSA algorithm to unmix the reconstructed data. MVSA is an endmember generation algorithm with outstanding performance, which is initialized by using the Vertex Component Analysis (VCA) [13] endmembers extraction result. After multispectral unmixing, the emission spectra can be derived. Then the concentration distributions of luminophor materials can be reconstructed by solving Eq. (1).

2.2. Principle of Compressive Sampling

Compared with the conventional methods, in compressive sampling, a signal can be recovered by far fewer samples under certain conditions. A detailed description of compressive sampling based single-pixel imaging can be found in Ref. [8]. Herein, the image of the sample object is represented by an $N \times 1$ vector x , which can be expressed as $x = \Psi\alpha$, where Ψ is an $N \times N$ representation basis matrix with vectors $\{\Psi_k\}$ as the columns and α is the $N \times 1$ vector composed of the coefficients of x in the expansion.

For most images of interest, only a small fraction of the coefficients in vector α are nonzero. By using CS, an object image can be reconstructed by M ($M < N$) linear measurements of the object image projected on a basis of M intensity patterns Φ_m ($m = 1, 2, \dots, M$) with an N -pixel resolution. The measurement can be expressed as $y = \Phi x$, where Φ is a $M \times N$ sampling matrix with each row a base vector Φ_m and y an $M \times 1$ vector representing M measurements obtained by a single-point detector.

The measurement process can be represented by

$$y = \Phi x = \Phi(\Psi\alpha) = (\Phi\Psi)\alpha = \Theta\alpha, \quad (2)$$

where Φ is a random projection matrix, and Ψ is a short-time Fourier basis.

To recover the image x from the random measurements y , a proper reconstruction algorithm must be used to solve Eq. (2). The best strategy is to perform the l_1 -norm minimization of α subject to Eq. (2). As most of the measurements are with noise, it is better to relax the constraints into

$$\min \|\alpha\|_{l_2} \text{ subject to } \|y - \Theta\alpha\|_{l_2} \leq \varepsilon, \quad (3)$$

where ε bounds the amount of noise in the data [9].

In this study, we use the NESTA solver [14] to reconstruct the image for each band. The NESTA algorithm is based on Nesterov's method and obeys the properties of speed, accuracy and flexibility. By using NESTA solver L times for L bands, an $L \times N$ multispectral image can be derived.

2.3. Postprocessing of CS Images before Spectral Extracting

Images obtained by means of CS typically contain random noise, which is more serious with a decreased number of measurements. The random noise dominates the background signal of the image and lowers the signal to noise ratio (SNR). For a spectral image with high SNR, the background of image can be ignored when performing spectral unmixing as the majority of the background value is close to zero. However, for spectral images acquired through CS, the background bears high noise and non-zero optical intensity value. This noise will deteriorate the results of spectral unmixing and the noise in background should be extracted and removed before performing multispectral unmixing. Herein, the spectral image can be treated as a two-dimensional optical intensity distribution, in which the maximum optical intensity is denoted by I_{\max} . During the process of multispectral unmixing, pixels with extreme low optical signal (less than 9.5% of I_{\max}) are removed, making it possible to perform spectral unmixing in a CS case. Here 9.5% is defined as the denoising factor. Enlarging the denoising factor can improve the SNR of the spectral image, however the cost of a reduced dynamic range of the image. For our fluorescent image, the choice of 9.5% as the denoising factor is a tradeoff between the accuracy of spectral unmixing and the dynamic range.

2.4. Similarity Metric

To evaluate the similarity between pure and reconstructed multispectral images, a distance metric proposed by Nascimento, spectral angle distance (SAD), is adopted [15]. SAD is expressed as

$$\text{SAD} = \text{COS}^{-1} \left(\frac{\alpha \cdot \beta}{\|\alpha\| * \|\beta\|} \right), \quad (4)$$

where α and β denote the pure spectrum and the extracted spectrum, respectively. Generally, if SAD is less than 0.1, the multispectral reconstruction's accuracy is acceptable and the extracted endmembers can be used for further applications [12].

3. SIMULATED RESULTS AND ANALYSIS

In our previously reported work we obtained spectral images of a mouse injected with fluorescent agent DTTC (Diethyl thioaldehyde tricarbocyanine iodide) in the nanoparticles [15]. A MaestroTM in-vivo imaging system (CRI, Woburn, Massachusetts) was used to acquire the original data, $M = [M_1, M_2]$

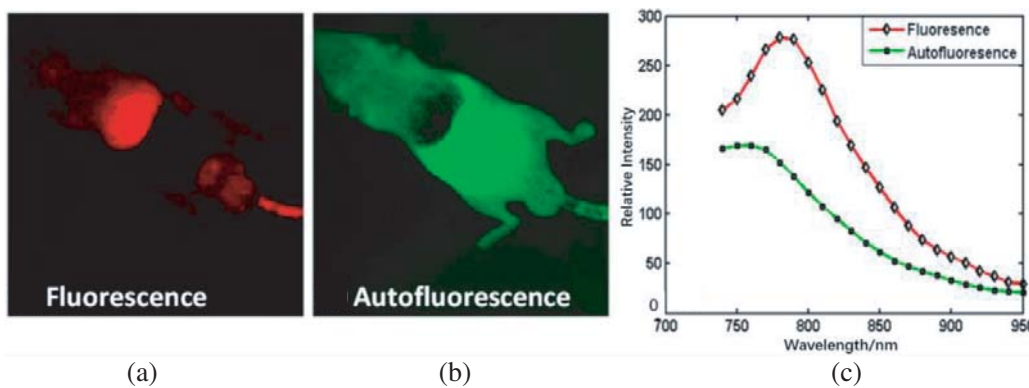


Figure 1. Original fluorescent distribution and spectra for a mouse injected with fluorescent agent DTTC (Diethyl thioaldehyde tricarbocyanine iodide). (a)–(b) Original distribution for fluorescence (DTTC) and autofluorescent material. (c) Fluorescence (DTTC) and autofluorescence spectra.

and $X = [X_1, X_2]$, where $M_{1,2}$ and $X_{1,2}$ represent the fluorescent spectra and fluorescent distributions for the DTTC and the autofluorescence. $M_{1,2}$ consist of 22 bands in a range of 740 nm to 950 nm. The original fluorescent spectra and distributions are shown in Fig. 1. The DTTC is concentrated in the liver due to the metabolic functions of the mouse. The top of the autofluorescence signal locates at the stomach, which is attributed to the food eaten by the mouse. By using the original data M and X , the MSI data Y can be derived by using Eq. (1).

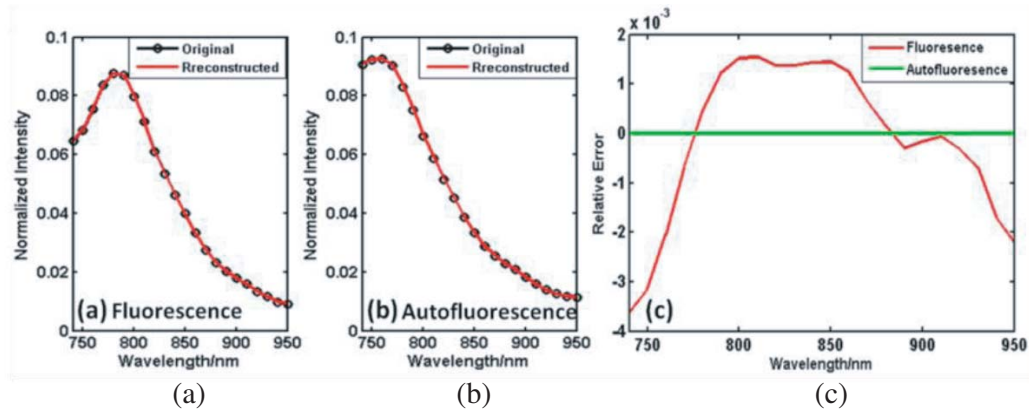


Figure 2. Spectral unmixing results by using MVSA algorithm. (a) Original and reconstructed DTTC fluorescence spectra. (b) Original and reconstructed autofluorescence spectra. (c) Relative errors between the original and reconstructed spectra.

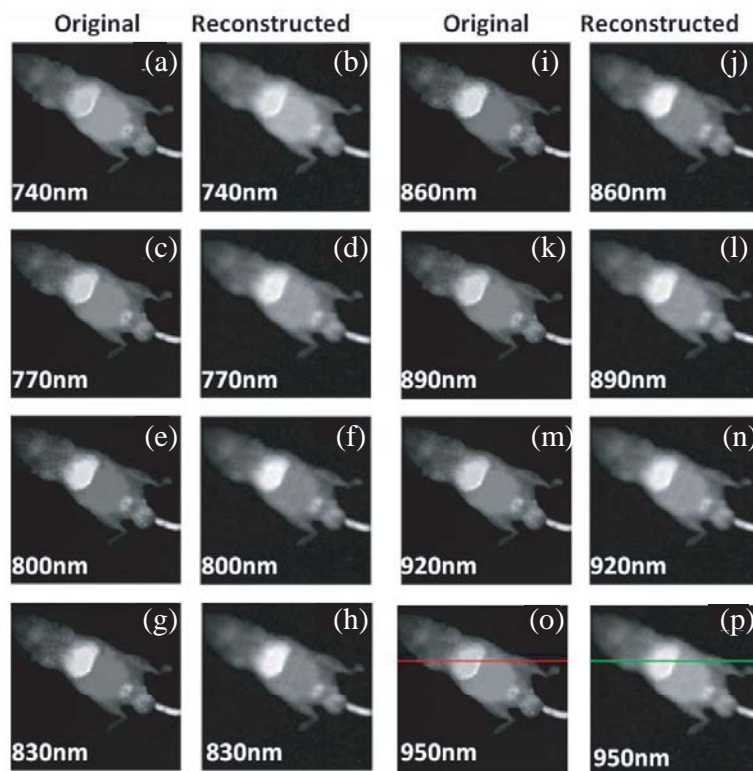


Figure 3. Multispectral image cube reconstructed by means of the CS algorithm at 8 of 22 wavelengths with a separation interval of 30 nm. The first and third columns present the original spectral images; the second and fourth columns present the reconstructed images accordingly. The reconstructed images have relatively larger background noise.

To validate the MVSA algorithm, the MSI data Y were treated as the sole input variables and processed by MVSA without any other prior knowledge and the results are represented as M_{est} . As shown in Figs. 2(a) and (b), the original spectra M and the reconstructed spectra M_{est} fit well. The relative errors are shown in Fig. 2(c). We observe that the MVSA relative error is less than 0.4% without any other prior knowledge autofluorescence spectra, showing the feasibility of using MVSA to perform spectral unmixing for mouse fluorescent imaging.

A recent work [10] has also demonstrated that multispectral images can be acquired sequentially through a CS based single pixel imaging scheme. The question is: can multispectral images acquired from this CS based single pixel imaging scheme be well spectral unmixed? In the following, we will numerically simulate MSI data acquired by CS based single pixel imaging and demonstrate the feasibility of unmixing the simulated MSI data.

The original MSI data Y is composed of multiple images, each of which with a spatial resolution of 128×128 pixels, represents a 2-D fluorescent distribution at one spectral band. For one image, a series of 128×128 random matrixes, whose elements are uniformly distributed in the range (0, 1) and binarized by a threshold value 0.5, was chosen as the random patterns. A CS measurement was performed by projecting one random pattern on one image and focusing the light of this projected image onto a single pixel detector. After repeating the measurement process T times, an intensity measurement sequence with T elements is acquired. As mentioned in Ref. [16], a higher compression rate leads to a reconstructed CS image with a lower SNR. Taken the SNR into account, through a series of pre-simulation, the number of CS measurements, T , was chosen to be 4096 ($4096 = 128 \times 128 \times 1/4$, i.e., a compression rate of 4:1). The above process can be numerically simulated, and through the $T \times 1$ simulated single pixel detection data, together with the random patterns, the NESTA solver can reconstruct the image. The images reconstructed using the NESTA solver as well as the original images are shown in Fig. 3. By using the CS method, the time to acquire multispectral images through the

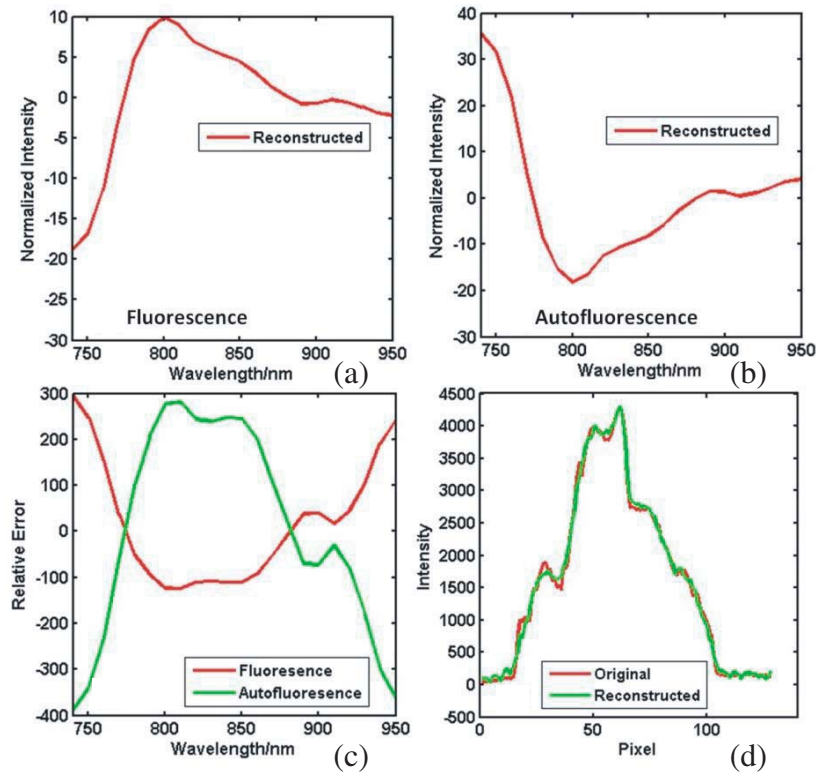


Figure 4. Endmember extraction results without handling noise of (a) DTTC fluorescence spectrum. (b) Autofluorescence spectrum. (c) Relative error for DTTC fluorescence and autofluorescence spectra. (d) The original and reconstructed optical intensity curves represent the line profiles in Fig. 3(o) and Fig. 3(p) respectively.

single pixel imaging scheme can be reduced by a quarter, however, at the expense of an added large background noise. As can be seen in Fig. 4(d), the reconstructed optical intensity curve, representing the line profile in Fig. 3(p) (950 nm), has relatively large background noise as compared to the original optical intensity curve corresponding to the line profile in Fig. 3(o). However, as can also be seen, the reconstructed images in Fig. 3 still clearly provides the information that the fluorescent agents are mostly accumulated in the liver indicating that it is feasible to use such a CS based single pixel

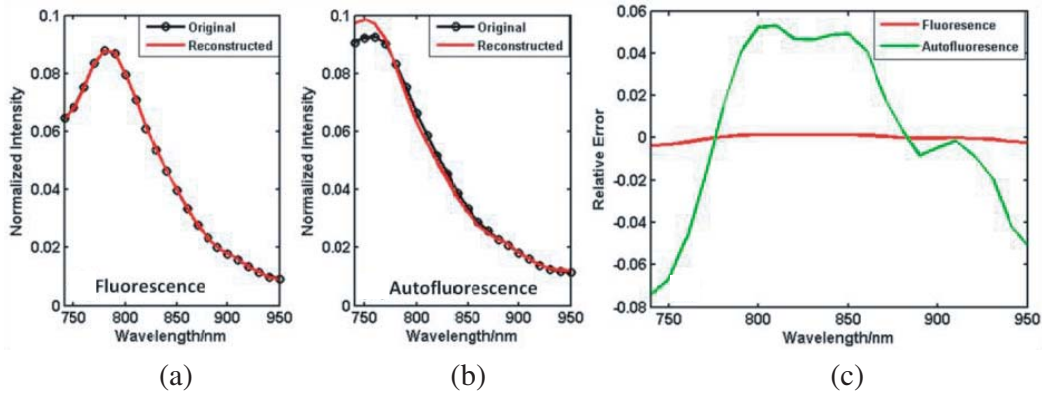


Figure 5. Spectral unmixing results from 25% measurements (with a compression ratio of 4:1) after CS. (a) original and reconstructed Fluorescence (DTTC) spectra. (b) Original and reconstructed autofluorescence spectra. (c) Relative error for fluorescence and autofluorescence spectra. The relative error between original and reconstructed autofluorescence spectra is lower than 8% and that for DTTC spectra is lower than 0.2%.

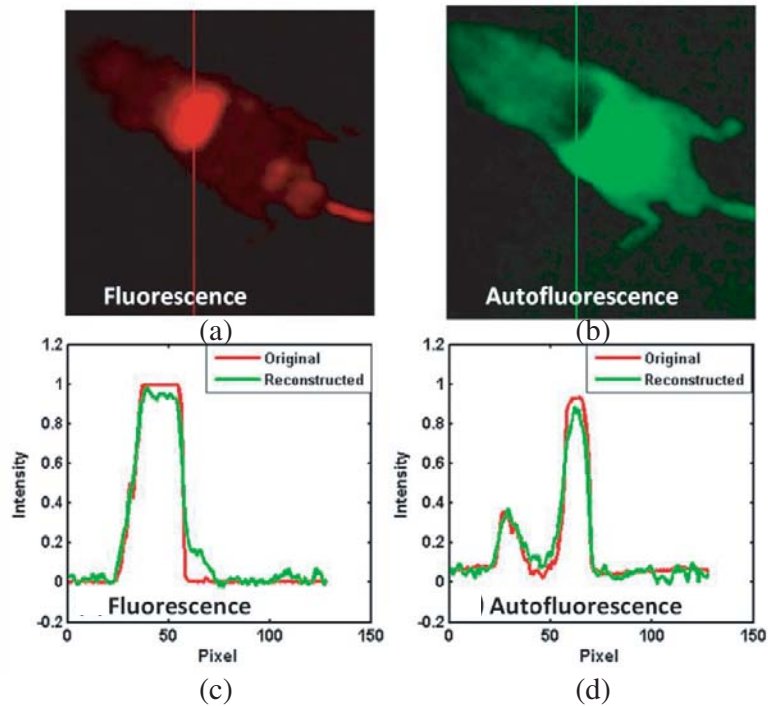


Figure 6. Reconstructed concentration distribution of (a) fluorescence (DTTC) and (b) autofluorescence. Reconstructed optical intensity curves of (c) and (d) represent the line profiles in (a) and (b) respectively. The original ones represent the corresponding line profiles (not marked) in Fig. 1(a) and Fig. 1(b) respectively.

imaging scheme for in-vivo fluorescence imaging in biomedical studies. This analysis is valid for other wavelengths.

The NESTA reconstructed images are still admixed with autofluorescence signals. In order to unmix the autofluorescence, the NESTA reconstructed images are further processed by using the MVSA algorithm. However, due to the large background noise in the spectral-images, the directly reconstructed spectra are not correct at all, which can be seen from the unreasonable negative values in the spectral curves as shown in Figs. 4(a) and (b).

As described in Section 2.3, to remove the background noise and obtain a better spectral unmixing result, pixels having extremely low optical signal strength (less than 9.5% of the I_{\max}) are set to be zero. After de-noising, the NESTA reconstructed images are processed by the MVSA algorithm again, and the new unmixing spectra are shown in Fig. 5. Compared with the unmixing spectra shown in Fig. 4, it is evident that the de-noising method can improve spectral unmixing result of CS images. The SADs for the reconstructed DTTC and autofluorescence spectra are 0.0026 and 0.0477 respectively. The reconstructed DTTC spectrum is a good fit to the original spectrum, having a relative error less than 0.2%. The reconstructed result of autofluorescence spectrum is, on the other hand, relatively poor, but even so, the relative error is still less than 8%. The main reason for this is due to the low intensity of autofluorescence, which makes it vulnerable to background noise. As can be seen in Fig. 6, there exists obvious background noise in the reconstructed autofluorescence image. From Fig. 6(c), we can see that, the reconstructed concentration distribution of the DTTC, which is the fluorescent signal of interest, agrees well with the original data with despite the presence of a high SNR.

4. CONCLUSION

In this paper we have presented a compressive sampling based imaging and unmixing scheme for multispectral data processing, which does not require any a priori knowledge of the endmember distribution. The method has applications in fluorescent imaging of small animals. Through the use of compressive sampling, the requirements on hardware design are less stringent than for traditional approaches. Currently, the work of this paper applies to when the signal of interest is comparable to the autofluorescence and the demand for resolution is not high, due to the denoising method of removing pixels under chosen threshold for background noise induced by compressive sampling. The numerical results presented in this paper clearly demonstrate the potential of this method to be able to extract essential spectral information in a precise manner. Extending this technique to situations with low signal to noise ratio is theoretically achievable since NESTA and MVSA have the capability to operate at high accuracy [12, 16], but the denoising procedure would require more sophistication. Compressive sampling unmixing, as a complement to standard unmixing techniques, has the potential to be applied in the real large-scale multispectral imaging applications in the future.

ACKNOWLEDGMENT

We would like to thank Wanrong Gao for insightful discussions. This work was supported by the Science and Technology Department of Zhejiang Province (2010R50007), the National Basic Research Program (973) of China (2011CB503700), Fundamental Research Funds for the Central Universities, Zhejiang Preferred funded postdoctoral scientific research project (BSH1401011) and the “111” Project.

REFERENCES

1. Jorgensen, K., J. Africano, K. Hamada, et al., “Physical properties of orbital debris from spectroscopic observations,” *Advances in Space Research*, Vol. 34, No. 5, 1021–1025, 2004.
2. Lin, R. P., B. R. Dennis, G. J. Hurford, et al., *The Reuven Ramaty High-energy Solar Spectroscopic Imager (RHESSI)*, Springer Netherlands, Berlin, 2003.
3. Pham, T. H., F. Bevilacqua, T. Spott, et al., “Quantifying the absorption and reduced scattering coefficients of tissue-like turbid media over a broad spectral range with noncontact Fourier-transform hyperspectral imaging,” *Applied Optics*, Vol. 39, No. 34, 6487–6497, 2000.

4. Keshava, N. and J. F. Mustard, "Spectral unmixing," *IEEE Signal Processing Magazine*, Vol. 19, No. 1, 44–57, 2002.
5. Zacharakis, G., R. Favicchio, A. Garofalakis, et al., "Spectral unmixing of multi-color tissue specific in vivo fluorescence in mice," *European Conference on Biomedical Optics. Optical Society of America*, 6626_8, 2007.
6. Xu, H. and B. W. Rice, "In-vivo fluorescence imaging with a multivariate curve resolution spectral unmixing technique," *Journal of Biomedical Optics*, Vol. 14, No. 6, 064011-064011–9, 2009.
7. Mansfield, J. R., K. W. Gossage, C. C. Hoyt, et al., "Autofluorescence removal, multiplexing, and automated analysis methods for in-vivo fluorescence imaging," *Journal of Biomedical Optics*, Vol. 10, No. 4, 041207-041207–9, 2005.
8. Duarte, M. F., M. A. Davenport, D. Takhar, et al., "Single-pixel imaging via compressive sampling," *IEEE Signal Processing Magazine*, Vol. 25, No. 2, 83, 2008.
9. Candès, E. J. and M. B. Wakin, "An introduction to compressive sampling," *IEEE Signal Processing Magazine*, Vol. 25, No. 2, 21–30, 2008.
10. Soldevila, F., E. Irlés, V. Durán, et al., "Single-pixel polarimetric imaging spectrometer by compressive sensing," *Applied Physics B*, Vol. 113, No. 4, 551–558, 2013.
11. Li, C., T. Sun, K. F. Kelly, et al., "A compressive sensing and unmixing scheme for hyperspectral data processing," *IEEE Transactions on Image Processing*, Vol. 21, No. 3, 1200–1210, 2012.
12. Shuai, T., X. Zhang, M. Zhang, et al., "Accuracy analysis of lunar mineral end members extraction using simulated Chang' E-1 IIM data," *Yaogan Xuebao — Journal of Remote Sensing*, Vol. 16, No. 6, 1205–1221, 2012.
13. Nascimento, J. M. P. and J. M. B. Dias, "Vertex component analysis: A fast algorithm to unmix hyperspectral data," *IEEE Transactions on Geoscience and Remote Sensing*, Vol. 43, No. 4, 898–910, 2005.
14. Becker, S., J. Bobin, and E. J. Candès, "NESTA: A fast and accurate first-order method for sparse recovery," *SIAM Journal on Imaging Sciences*, Vol. 4, No. 1, 1–39, 2011.
15. Zhan, Y., J. Qian, D. Wang, et al., "Multifunctional gold nanorods with ultrahigh stability and tunability for in vivo fluorescence imaging, SERS detection, and photodynamic therapy," *Angewandte Chemie International Edition*, Vol. 52, No. 4, 1148–1151, 2013.
16. Studer, V., J. Bobin, M. Chahid, et al., "Compressive fluorescence microscopy for biological and hyperspectral imaging," *Proceedings of the National Academy of Sciences*, Vol. 109, No. 26, E1679–E1687, 2012.